JOURNAL OF GUIDANCE, CONTROL, AND DYNAMICS
Vol. 30, No. 5, September–October 2007

Optimal Control of Sensor Threshold for Autonomous Wide-Area-Search Munitions

Brian A. Kish,* David R. Jacques,† and Meir Pachter‡
U.S. Air Force Institute of Technology, Wright–Patterson Air Force Base, Ohio 45433

DOI: 10.2514/1.18782

The optimal employment of autonomous wide-area-search munitions is addressed. The scenario considered involves an airborne munition searching a battle space for stationary targets in the presence of false targets. Targets are modeled with uniform, Poisson, and normal distributions. False targets are modeled with Poisson distributions. All relevant parameters can be extracted from intelligence information on the enemy's order of battle and the sensor performance specification. Analytic weapon-effectiveness measures are derived using applied probability theory. The effectiveness measures derived in this paper handle time-varying parameters that characterize the battle-space environment and the performance of the munition's sensor. This allows the formulation and solution of optimization problems that maximize the probability of a target attack while constraining the probability of a false-target attack. Optimal schedules for controlling the sensor threshold during the flight are derived and compared with the optimal constant-threshold results. An increase in weapon effectiveness is demonstrated when the sensor threshold is dynamically controlled during the flight.

Nomenclature

$\mathcal{C}$	=	events involving classified encounters
c	=	receiver operating characteristic curve parameter
$\mathcal{E}$	=	events involving encounters
H	=	Hamiltonian
L	=	integrand of cost functional
P_{FTA}	=	probability of a false-target attack
P_{FTE}	=	probability of a false-target encounter
P_{FTR}	=	probability of a false-target report given a false-target encounter
P_{TA}	=	probability of a target attack
P_{TE}	=	probability of a target encounter
P_{TR}	=	probability of a target report given a target encounter
R	=	terminal radius
r	=	search radius
T	=	mission duration
t	=	time
v	=	velocity
w	=	swath width
Y	=	probability of a false-target attack
y	=	dynamic Poisson parameter
z	=	probability of a target attack when no false targets exist
α	=	false-target density
β	=	target density
λ	=	costate
μ	=	rate of encounters
ρ	=	radius
σ	=	standard deviation
τ	=	time

Presented as Paper 6190 at the AIAA Guidance, Navigation, and Control Conference, San Francisco, CA, 15–18 August 2005; received 12 July 2005; revision received 7 November 2005; accepted for publication 31 January 2006.

*Major, U.S. Air Force, 2950 Hobson Way. AIAA Senior Member.
†Assistant Professor, Department of Aeronautical Engineering, 2950 Hobson Way. AIAA Associate Fellow.
‡Professor, Department of Electrical Engineering, 2950 Hobson Way. AIAA Associate Fellow.

I. Introduction

SEVERAL types of autonomous wide-area-search munitions are currently being developed for high-risk air-to-ground missions. These airborne munitions will deploy to a battle space and autonomously search, detect, classify, and attack targets. In this paper, we acknowledge the presence of false targets in the battle space and derive analytic weapon-effectiveness measures based on target and false-target probability distributions as well as the munition's sensor characteristics. All relevant parameters can be extracted from intelligence information on the enemy's order of battle and the sensor performance specification. This has been done for wide-area-search munitions in the past; however, the problem parameters were assumed constant [1]. We now generalize the results of [1] to handle time-varying parameters. This then allows one to address the optimal control of the sensor threshold to maximize the probability of a target attack without unduly increasing the probability of a false-target attack. The latter is crucial, we believe, for making autonomous operation acceptable to the war fighter.

The battle-space geometries considered are rectangular and circular. In a rectangular battle space of length l and width w, the munition covers the area using a constant velocity v starting at initial time $t = 0$ and ending at final time $t = T$. The sensor footprint is rectangular with swath width w and incremental swath length $v\,\mathrm{d}t$, as shown in Fig. 1. Hence, the munition covers the battle space in one sweep. In a circular battle space of radius R, the munition covers the area using concentric annuli of thickness $\mathrm{d}r$, as shown in Fig. 2. The munition starts at the origin and progresses outward. This method of concentric annuli approximates an outward-spiral search pattern.

The scenarios considered involve one munition searching for stationary targets among a field of false targets. In operations research, the distribution of false targets in a battle space is often modeled using a Poisson distribution [1–3]. We consider three scenarios involving a Poisson field of false targets. The first scenario addresses the case when a single target may appear anywhere within a rectangular battle space with equal probability, thus the target encounter is modeled with a uniform distribution. The second scenario addresses the case when target encounters occur at an expected rate in a rectangular battle space, thus target encounters are modeled with a Poisson distribution. Finally, the third scenario addresses the case when specific information is available about a target (i.e., position coordinates with some error). We model the target with a circular normal distribution and define the corresponding battle space is defined as circular. In all three scenarios, flight altitude and speed are constant, and the munition covers the entire search area. The approach used in this research

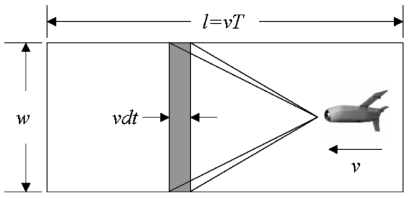

Fig. 1 Rectangular search area.

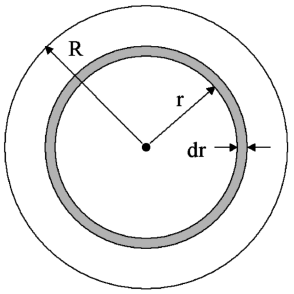

Fig. 2 Circular search area.

provides analytic results can be used to verify simulations. The analytic results also provide insight into the trade space.

A. Sensor Performance

When a sensor encounters an object, it compares the image to a database and either declares the object a target or a false target. Sensor performance is judged by how often the sensor is correct. The probability of a target report, P_{TR}, is the probability that the sensor will correctly report a target when given a target encounter. The probability of a false-target report, P_{FTR}, is the probability that the sensor will correctly report a false target when a false target is encountered. Together, P_{TR} and P_{FTR} determine the entries of the "confusion matrix" shown in Table 1, which can be used to determine the outcome of a random draw each time an object is encountered. The parameters P_{TR} and P_{FTR} characterize the sensor's performance and are not independent. They are linked by a receiver operating characteristic (ROC) curve. A mathematical representation ROC curve produces a graph of true positive fraction P_{TR} versus false positive fraction $(1 - P_{\mathrm{FTR}})$ that starts at (0,0), then monotonically increases to (1,1). We use the ROC curve model adapted from [4]:

$$(1 - P_{\mathrm{FTR}}) = \frac{P_{\mathrm{TR}}}{(1 - c)P_{\mathrm{TR}} + c} \tag{1}$$

where the nondimensional scalar parameter c depends on the sensor and data processing algorithm. It also depends on the munition speed (dwell time) and engagement geometry, which includes flight altitude and look angle. Systems with $c \in [1, \infty)$ are considered. These systems are correct at least half of the time. A family of ROC curves parameterized by c is shown in Fig. 3. As c increases, the ROC improves. As $c \to \infty$, the area under the curve approaches unity, indicating perfect identification. We will use $c = 100$ for all examples in this paper.

The operating point on a ROC curve is the ordered pair $[(1 - P_{\mathrm{FTR}}), P_{\mathrm{TR}}]$. For a given sensor and algorithm, the operating point is determined by the sensor's threshold. Setting the threshold is tantamount to setting P_{TR}. The value for $1 - P_{\mathrm{FTR}}$ is calculated using Eq. (1). Given a ROC curve, our goal is finding the optimal P_{TR}: either constant or as a function of time or space.

Table 1 Confusion matrix

	Encountered object	
Declared object	Target	False target
Target	P_{TR}	$1 - P_{\mathrm{FTR}}$
False target	$1 - P_{\mathrm{TR}}$	P_{FTR}

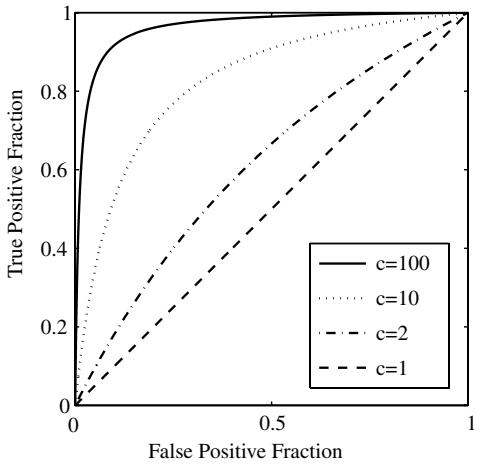

Fig. 3 Family of ROC curves.

B. Optimal Control Problem Formulation

An operator wants the probability of a target attack, P_{TA}, in a battle space to be high and the probability of a false-target attack, P_{FTA}, to be low. Therefore, P_{TA} and P_{FTA} become weapon-effectiveness measures. Unfortunately, increasing P_{TR} by reducing sensor threshold with a view to *increase* P_{TA} also increases $1 - P_{\mathrm{FTR}}$ and, consequently, P_{FTA}. This state of affairs is modeled by the ROC. Thus, the operator's objectives are competing and a tradeoff situation arises. To ensure that P_{FTA} stays low, a constraint is imposed on it. The optimization problem statement is then

Maximize:

$$P_{\mathrm{TA}}$$

Subject to:

$$P_{\mathrm{FTA}} \leq P_{\mathrm{FTA}_{\max}}$$

where $P_{\mathrm{FTA}_{\max}}$ is set by the operator.

To solve the posed optimization problem, expressions are developed for P_{TA} and P_{FTA} for the considered scenarios. This involves integrating probability density functions parameterized by P_{TR}, velocity, and search width, as well as data on the battle-space environment concerning target and false-target densities. The latter are obtained from knowledge of the order of battle. We assume that velocity and search width are constant, and so our decision variable is P_{TR}. We use the explicit ROC model given by Eq. (1); however, the discerned trends will apply to any ROC. With an inequality constraint, we first solve the unconstrained problem and check if the constraint is met. If $P_{\mathrm{FTA}} < P_{\mathrm{FTA}_{\max}}$, we also impose the constrained $P_{\mathrm{TR}} \in [0, 1]$.

To provide a benchmark, we solve the constant-threshold problems first. Holding P_{TR} constant yields a static (parameter) optimization problem, and closed-form solutions are possible. More important from an operational point of view, using a constant sensor threshold (i.e., a constant P_{TR}) is the easiest way to employ a wide-area-search munition. The dynamic-threshold problem and, consequently, the dynamic-P_{TR} problem can be formulated as a textbook optimal control problem [5,6].

II. Scenario 1: One Uniformly Distributed Target and a Poisson Field of False Targets

The scenario when one target is uniformly distributed over a battle space among a Poisson field of false targets is considered. With an expendable munition, the probability of an attack occurring during the time interval $[t, t + \mathrm{d}t]$ is conditioned on the probability of no

attacks occurring before t. The probabilities in [1] were calculated assuming constant parameters. We rederive the probabilities to be time-varying parameters.

In the infinitesimal interval $[t, t + \mathrm{d}t]$, such as that shown in Fig. 1, three events can occur: a target is attacked, a false target is attacked, or an attack does not occur. Assuming that no attacks occurred before t, the probability of a target attack occurring in the time interval $[t, t + \mathrm{d}t]$ is

$$P_{\mathrm{TR}}(t) \cdot P_{\mathrm{TE}}(t) \tag{2}$$

where $P_{\mathrm{TE}}(t)$ is the probability of a target encounter in the infinitesimal footprint. Similarly, the probability of a false-target attack is

$$[1 - P_{\mathrm{FTR}}(t)] \cdot P_{\mathrm{FTE}}(t) \tag{3}$$

where $P_{\mathrm{FTE}}(t)$ is the probability of a false-target encounter in the infinitesimal footprint. Finally, the probability of no attack occurring during $[t, t + \mathrm{d}t]$ is

$$[1 - P_{\mathrm{TR}}(t)] \cdot P_{\mathrm{TE}}(t) + P_{\mathrm{FTR}}(t) \cdot P_{\mathrm{FTE}}(t) + 1 - P_{\mathrm{TE}} - P_{\mathrm{FTE}} \tag{4}$$

The classification probabilities $P_{\mathrm{TR}}(t)$, $1 - P_{\mathrm{TR}}(t)$, $P_{\mathrm{FTR}}(t)$, and $1 - P_{\mathrm{FTR}}(t)$ are specified. The encounter probabilities $P_{\mathrm{TE}}(t)$ and $P_{\mathrm{FTE}}(t)$ are determined from the respective target and false-target distributions. For one uniformly distributed target,

$$P_{\mathrm{TE}}(t) = \frac{w(t)v(t)\,\mathrm{d}t}{A_s} \tag{5}$$

where the battle space or area searched A_s is

$$A_s \equiv \int_0^T w(t)v(t)\,\mathrm{d}t \tag{6}$$

For a Poisson field of false targets,

$$P_{\mathrm{FTE}}(t) = \alpha(t)w(t)v(t)\,\mathrm{d}t \tag{7}$$

where $\alpha(t)$ is the mean false-target density at time t. Indeed, the false-target density in the battle space need not be constant and could vary from place to place, thereby being time-dependent.

Formulas for the probabilities of no previous attacks before t are now given. Detailed derivations are given in the Appendix. For one uniformly distributed target, the probability of no target attack occurring before time t is

$$P_{\overline{\mathrm{TA}}}(t) = 1 - \frac{1}{A_s}\int_0^t P_{\mathrm{TR}}(\tau)w(\tau)v(\tau)\,\mathrm{d}\tau \tag{8}$$

For a Poisson field of false targets with density $\alpha(\tau)$, $0 \le \tau \le t$, the probability of no false-target attacks occurring before time t is

$$P_{\overline{\mathrm{FTA}}}(t) = e^{-\int_0^t [1 - P_{\mathrm{FTR}}(\tau)]\alpha(\tau)w(\tau)v(\tau)\,\mathrm{d}\tau} \tag{9}$$

The probability of a target attack can now be calculated as

$$\begin{aligned} P_{\mathrm{TA}} &= \int_0^T P_{\mathrm{TR}}(t) \cdot P_{\mathrm{TE}}(t) \cdot P_{\overline{\mathrm{FTA}}}(t) \\ &= \int_0^T \frac{1}{A_s} P_{\mathrm{TR}}(t)w(t)v(t)e^{-\int_0^t [1 - P_{\mathrm{FTR}}(\tau)]\alpha(\tau)w(\tau)v(\tau)\,\mathrm{d}\tau}\,\mathrm{d}t \end{aligned} \tag{10}$$

and the probability of a false-target attack is

$$\begin{aligned} P_{\mathrm{FTA}} &= \int_0^T [1 - P_{\mathrm{FTR}}(t)] \cdot P_{\mathrm{FTE}}(t) \cdot P_{\overline{\mathrm{TA}}}(t) \cdot P_{\overline{\mathrm{FTA}}}(t) \\ &= \int_0^T [1 - P_{\mathrm{FTR}}(t)]\alpha(t)w(t)v(t) \\ &\times \left(1 - \int_0^t \frac{1}{A_s} P_{\mathrm{TR}}(\tau)w(\tau)v(\tau)\,\mathrm{d}\tau\right) e^{-\int_0^t [1 - P_{\mathrm{FTR}}(\tau)]\alpha(\tau)w(\tau)v(\tau)\,\mathrm{d}\tau}\,\mathrm{d}t \end{aligned} \tag{11}$$

We now address the problem of finding the optimal $P_{\mathrm{TR}}(t)$, $0 \le t \le T$, assuming that w, v, and α are constant. Recall that $P_{\mathrm{FTR}}(t)$ is determined from $P_{\mathrm{TR}}(t)$ and related by the ROC.

A. Constant Threshold

When the sensor threshold is constant during the flight, P_{TR} and, consequently, P_{FTR} are constant, and we get closed-form solutions when evaluating the integrals in Eq. (10) and (11). The probability of a target attack is

$$P_{\mathrm{TA}} = P_{\mathrm{TR}} \frac{1 - e^{-(1 - P_{\mathrm{FTR}})\alpha wvT}}{(1 - P_{\mathrm{FTR}})\alpha wvT} \tag{12}$$

and the probability of a false-target attack is

$$P_{\mathrm{FTA}} = 1 - P_{\mathrm{TA}} - (1 - P_{\mathrm{TR}})e^{-(1 - P_{\mathrm{FTR}})\alpha wvT} \tag{13}$$

We invoke the ROC model in Eq. (1), which relates P_{FTR} to P_{TR} and reduces the problem to a one-dimensional search for P^*_{TR}. We maximize P_{TA} subject to $P_{\mathrm{FTA}} \le P_{\mathrm{FTA}_{\max}}$.

To show an example, we provide values for the constants c, w, v, α, and T; units are time units. Assuming that $c = 100$, $\alpha wv = 50$ (1/time), and $T = 0.5$ (time), we plot the outcome probabilities versus P_{TR}. Figure 4 shows that the best unconstrained solution is $P^*_{\mathrm{TR}_u} = 0.723$ with a corresponding $P^*_{\mathrm{TA}_u} = 0.535$ and $P^*_{\mathrm{FTA}_u} = 0.318$. The subscript u is used to denote unconstrained solutions. If we bound P_{FTA} by $P_{\mathrm{FTA}_{\max}} = 0.2$, the best constrained solution is $P^*_{\mathrm{TR}} = 0.563$ with a corresponding $P^*_{\mathrm{TA}} = 0.483$. In Fig. 4, the outcome probability functions are smooth and well-behaved. The function for P_{TA} has only one peak and never crosses the line when $P_{\mathrm{TA}} = P_{\mathrm{TR}}$. The function for P_{FTA} is monotonically increasing in P_{TR}, and so any constrained solution will be unique. Finally, the function for the probability of no attack occurring is monotonically decreasing in P_{TR}, as expected.

We solved the constant-threshold optimization problem for a number of $P_{\mathrm{FTA}_{\max}}$ values and generated a plot of P^*_{TR} versus $P_{\mathrm{FTA}_{\max}}$. Figure 5 illustrates the sensitivity of the solution to changes in the upper bound $P_{\mathrm{FTA}_{\max}}$. For $P_{\mathrm{FTA}_{\max}} > 0.32$, the unconstrained solution is used.

B. Dynamic Threshold

When P_{TR} and, consequently, P_{FTR} are dynamic, we recognize that an optimal control problem is on hand. We introduce the state variables

$$x = \int_0^t \alpha wv[1 - P_{\mathrm{FTR}}(\tau)]\,\mathrm{d}\tau \tag{14}$$

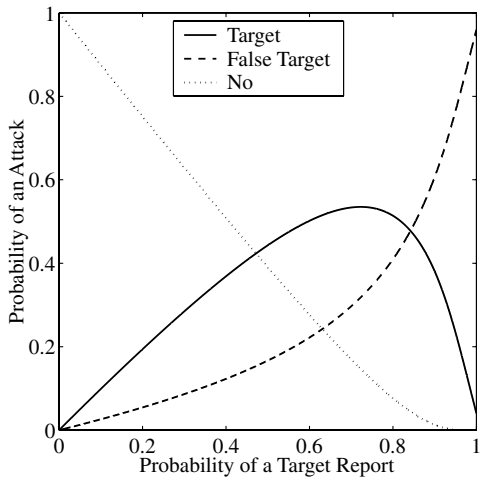

Fig. 4 Scenario involves one uniformly distributed target among a Poisson field of false targets; probability of a target report is constant throughout the flight; $c = 100$, $\alpha wv = 50$ (1/time), and $T = 0.5$ (time).

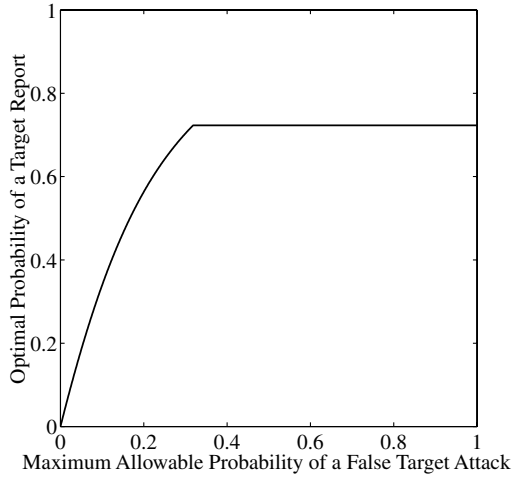

Fig. 5 Scenario involves one uniformly distributed target among a Poisson field of false targets; probability of a target report is constant throughout the flight; $c = 100$, $\alpha wv = 50$ (1/time), and $T = 0.5$ (time).

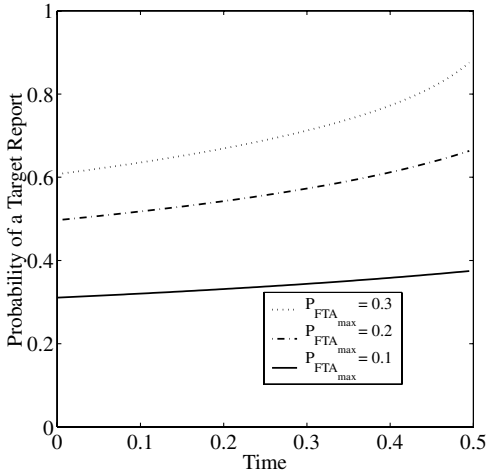

Fig. 6 Scenario involves one uniformly distributed target among a Poisson field of false targets; $c = 100$, $\alpha wv = 50$ (1/time), and $T = 0.5$ (time).

$$y = \int_0^t \frac{1}{T} P_{\mathrm{TR}}(\tau)\,\mathrm{d}\tau \tag{15}$$

$$z = \int_0^t \alpha wv[1 - P_{\mathrm{FTR}}(\tau)][1 - y(\tau)]e^{-x(\tau)}\,\mathrm{d}\tau \tag{16}$$

and the cost functional integrand L is

$$L = -\frac{1}{T} P_{\mathrm{TR}}(t)e^{-x(t)} \tag{17}$$

Obviously,

$$P_{\mathrm{TA}} = -\int_0^T L[P_{\mathrm{TR}}(t), x(t)]\,\mathrm{d}t \tag{18}$$

The state equations are

$$\dot{x} = \alpha wv[1 - P_{\mathrm{FTR}}(t)] \tag{19}$$

$$\dot{y} = \frac{1}{T} P_{\mathrm{TR}}(t) \tag{20}$$

$$\dot{z} = \alpha wv[1 - P_{\mathrm{FTR}}(t)][1 - y(t)]e^{-x(t)} \tag{21}$$

After applying Eq. (1) for the ROC model, the Hamiltonian H becomes

$$H = (\lambda_y - e^{-x})\frac{1}{T} P_{\mathrm{TR}} + \alpha wv \frac{P_{\mathrm{TR}}}{(1-c)P_{\mathrm{TR}} + c}[\lambda_x + \lambda_z(1-y)e^{-x}] \tag{22}$$

and the costate differential equations become

$$\dot{\lambda}_x = \lambda_z \alpha wv \frac{P_{\mathrm{TR}}}{(1-c)P_{\mathrm{TR}} + c}(1-y)e^{-x} - \frac{1}{T} P_{\mathrm{TR}} e^{-x} \tag{23}$$

$$\dot{\lambda}_y = \lambda_z \alpha wv \frac{P_{\mathrm{TR}}}{(1-c)P_{\mathrm{TR}} + c} e^{-x} \tag{24}$$

$$\dot{\lambda}_z = 0 \tag{25}$$

Taking the partial derivative of H with respect to the decision variable P_{TR}, we get

$$\frac{\partial H}{\partial P_{\mathrm{TR}}} = (\lambda_y - e^{-x})\frac{1}{T} + \frac{[\lambda_x + \lambda_z(1-y)e^{-x}]\alpha wvc}{[(1-c)P_{\mathrm{TR}} + c]^2} \tag{26}$$

Solving $\partial H / \partial P_{\mathrm{TR}} = 0$, the optimal control is

$$P^*_{\mathrm{TR}}(t) = \left(c \pm \sqrt{\frac{\{\lambda_x(t) + \lambda_z[1 - y(t)]e^{-x(t)}\}\alpha wvcT}{[e^{-x(t)} - \lambda_y(t)]}} \right) \Big/ (c-1) \tag{27}$$

Only the minus root is of interest, because the plus root always puts P_{TR} outside of $[0, 1]$. We are also interested in the optimal unconstrained solution $P^*_{\mathrm{TR}_u}$, which is

$$P^*_{\mathrm{TR}_u}(t) = \frac{c - \sqrt{\lambda_x(t)\alpha wvcTe^{x(t)}}}{c-1} \tag{28}$$

Taking the derivative of Eq. (28) with respect to t gives

$$\dot{P}^*_{\mathrm{TR}_u}(t) = \sqrt{\frac{\alpha wve^{-x(t)}}{4cT\lambda_x(t)}}[P^*_{\mathrm{TR}_u}(t)]^2 > 0 \tag{29}$$

Therefore, $P^*_{\mathrm{TR}_u}$ is monotonically increasing. At the terminal point at which $\lambda_x(T) = 0$, $P^*_{\mathrm{TR}_u}(T) = (c/c-1) > 1$. Thus, the constraint $P_{\mathrm{TR}} \in [0, 1]$ becomes active before the end and remains active until time T. This represents, for the unconstrained problem, a "go for broke" tactic in the end game.

Assuming that $c = 100$, $\alpha wv = 50$ (1/time), and $T = 0.5$ (time), we solved the constrained problem for a number of $P_{\mathrm{FTA}_{\max}}$ values. Figure 6 shows optimal solutions as a function of time for three values of $P_{\mathrm{FTA}_{\max}}$. As $P_{\mathrm{FTA}_{\max}}$ decreases, the optimal solution flattens out, approaching a constant-threshold solution.

We compare the objective function values of the dynamic solutions with those of the constant solutions. Figure 7 shows, for the assumed parameters, that the optimal dynamic solution is, at most, 3.4% better than the optimal constant solution. Depending on the application, this improvement may or may not be worth the added complexity.

III. Scenario 2: Poisson Fields of Targets and False Targets

The scenario when targets are also modeled with a Poisson distribution is considered. For this scenario, the battle space consists of a Poisson field of targets and a Poisson field of false targets. The

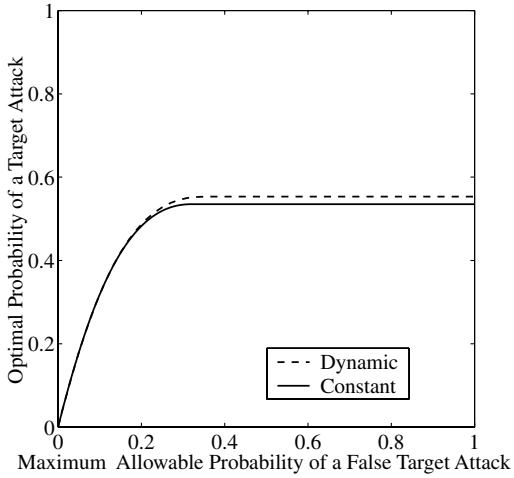

Fig. 7 Scenario involves one uniformly distributed target among a Poisson field of false targets;. $c = 100$, $\alpha wv = 50$ (1/time), and $T = 0.5$ (time).

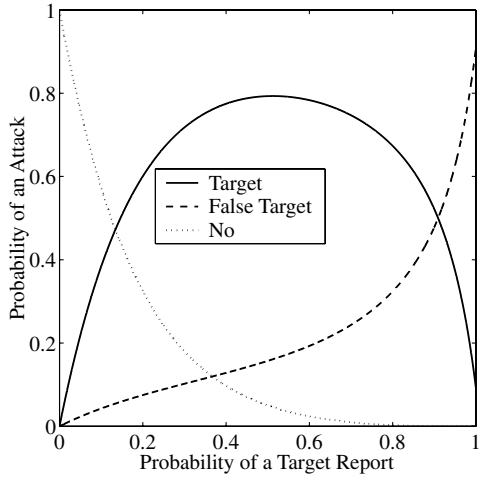

Fig. 8 Scenario involves a Poisson field of targets and a Poisson field of false targets; probability of a target report is constant throughout the flight; $c = 100$, $w = 0.2$ (distance), $v = 50$ (distance/time), $\alpha = 10$ (1/distance^2), $\beta = 1$ (1/distance^2), and $T = 0.5$ (time).

derivation of probabilities is similar to the previous scenario, with the following changes. For a Poisson field of targets,

$$P_{\mathrm{TE}}(t) = \beta(t)w(t)v(t)\,\mathrm{d}t \tag{30}$$

where $\beta(t)$ is the mean target density at time t. The probability of no target attacks occurring before time t is

$$P_{\overline{\mathrm{TA}}}(t) = e^{-\int_0^t P_{\mathrm{TR}}(\tau)\beta(\tau)w(\tau)v(\tau)\,\mathrm{d}\tau} \tag{31}$$

The probability of a target attack can now be calculated as

$$\begin{aligned} P_{\mathrm{TA}} &= \int_0^T P_{\mathrm{TR}}(t)\cdot P_{\mathrm{TE}}(t)\cdot P_{\overline{\mathrm{TA}}}(t)\cdot P_{\overline{\mathrm{FTA}}}(t) \\ &= \int_0^T P_{\mathrm{TR}}(t)\beta(t)w(t)v(t) \\ &\quad\times e^{-\int_0^t\{[1-P_{\mathrm{FTR}}(\tau)]\alpha(\tau)+P_{\mathrm{TR}}(\tau)\beta(\tau)\}w(\tau)v(\tau)\,\mathrm{d}\tau}\,\mathrm{d}t \end{aligned} \tag{32}$$

and the probability of a false-target attack is

$$\begin{aligned} P_{\mathrm{FTA}} &= \int_0^T [1-P_{\mathrm{FTR}}(t)]\cdot P_{\mathrm{FTE}}(t)\cdot P_{\overline{\mathrm{TA}}}(t)\cdot P_{\overline{\mathrm{FTA}}}(t) \\ &= \int_0^T [1-P_{\mathrm{FTR}}(t)]\alpha(t)w(t)v(t) \\ &\quad\times e^{-\int_0^t\{[1-P_{\mathrm{FTR}}(\tau)]\alpha(\tau)+P_{\mathrm{TR}}(\tau)\beta(\tau)\}w(\tau)v(\tau)\,\mathrm{d}\tau}\,\mathrm{d}t \end{aligned} \tag{33}$$

The parameters w, v, α, and β are constant.

A. Constant Threshold

When P_{TR} and, consequently, P_{FTR} are constant, we get closed-form solutions when evaluating the integrals in Eqs. (32) and (33). The probability of a target attack is

$$P_{\mathrm{TA}} = \frac{P_{\mathrm{TR}}\beta}{(1-P_{\mathrm{FTR}})\alpha + P_{\mathrm{TR}}\beta}\{1-e^{-[(1-P_{\mathrm{FTR}})\alpha+P_{\mathrm{TR}}\beta]wvT}\} \tag{34}$$

and the probability of a false-target attack is

$$P_{\mathrm{FTA}} = 1 - P_{\mathrm{TA}} - e^{-[(1-P_{\mathrm{FTR}})\alpha+P_{\mathrm{TR}}\beta]wvT} \tag{35}$$

To show an example, values must be provided for the various parameters; units are time and distance units. Invoking the ROC model in Eq. (1) and assuming that $c = 100$, $w = 0.2$ (distance), $v = 50$ (distance/time), $\alpha = 10$ (1/distance^2), $\beta = 1$ (1/distance^2), and $T = 0.5$ (time), the outcome probabilities are plotted versus P_{TR}. Figure 8 shows that the best unconstrained solution is $P^*_{\mathrm{TR}_u} = 0.513$ with a corresponding $P^*_{\mathrm{TA}_u} = 0.793$ and $P^*_{\mathrm{FTA}_u} = 0.161$. If we bound P_{FTA} by $P_{\mathrm{FTA}_{\max}} = 0.1$, the best constrained solution is $P^*_{\mathrm{TR}} = 0.292$ with a corresponding $P^*_{\mathrm{TA}} = 0.711$.

Like the previous scenario, the function for P_{TA} has only one peak. Unlike the previous scenario, the values of α and β can skew the function for P_{TA} above or below the line when $P_{\mathrm{TA}} = P_{\mathrm{TR}}$. However, the function for P_{FTA} is still monotonically increasing; thus, any constrained solution will be unique.

B. Dynamic Threshold

When P_{TR} and, consequently, P_{FTR} are dynamic, we introduce the state variables

$$x = \int_0^t \{[1-P_{\mathrm{FTR}}(\tau)]\alpha + P_{\mathrm{TR}}(\tau)\beta\}wv\,\mathrm{d}\tau \tag{36}$$

$$z = \int_0^t [1-P_{\mathrm{FTR}}(\tau)]\alpha wv e^{-x(\tau)}\,\mathrm{d}\tau \tag{37}$$

and L is

$$L = -P_{\mathrm{TR}}(t)\beta wv e^{-x(t)} \tag{38}$$

Because both targets and false targets have Poisson distributions, the state x represents a combined dynamic Poisson parameter; hence there is no need for a separate y state. The state equations are

$$\dot{x} = \{[1-P_{\mathrm{FTR}}(t)]\alpha + P_{\mathrm{TR}}(t)\beta\}wv \tag{39}$$

$$\dot{z} = [1-P_{\mathrm{FTR}}(t)]\alpha wv e^{-x(t)} \tag{40}$$

After applying Eq. (1) for the ROC model, the Hamiltonian becomes

$$H = (\lambda_x - e^{-x})P_{TR}\beta wv + (\lambda_x + \lambda_z e^{-x})\alpha wv\frac{P_{\mathrm{TR}}}{(1-c)P_{\mathrm{TR}}+c} \tag{41}$$

and the costate differential equations become

$$\dot{\lambda}_x = [\lambda_z\alpha\frac{P_{\mathrm{TR}}}{(1-c)P_{\mathrm{TR}}+c} - P_{\mathrm{TR}}\beta]wve^{-x} \tag{42}$$

$$\dot{\lambda}_z = 0 \tag{43}$$

Taking the partial derivative of H with respect to the decision variable P_{TR} gives

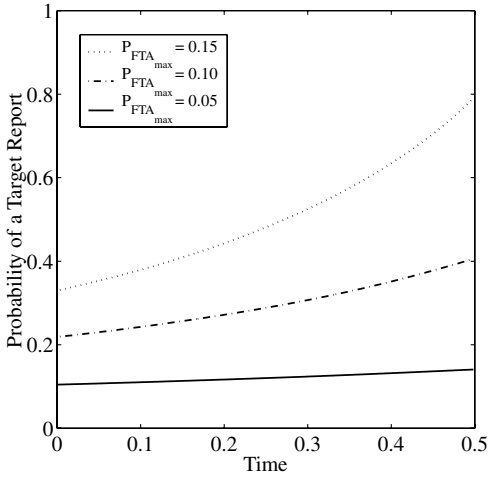

Fig. 9 Scenario involves a Poisson field of targets and a Poisson field of false targets; $c = 100$, $w = 0.2$ (distance), $v = 50$ (distance/time), $\alpha = 10$ (1/distance^2), $\beta = 1$ (1/distance^2), and $T = 0.5$ (time).

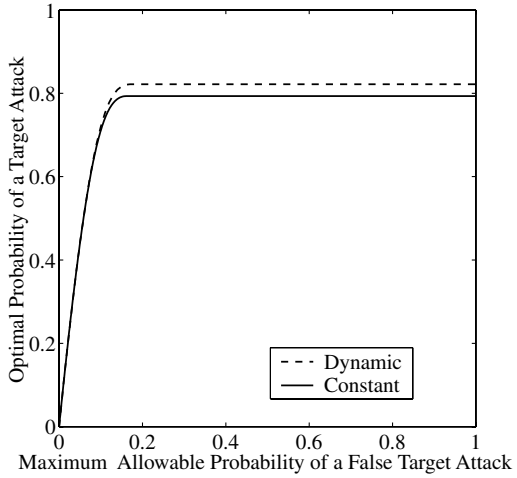

Fig. 10 Scenario involves a Poisson field of targets and a Poisson field of false targets; $c = 100$, $w = 0.2$ (distance), $v = 50$ (distance/time), $\alpha = 10$ (1/distance^2), $\beta = 1$ (1/distance^2), and $T = 0.5$ (time).

$$\frac{\partial H}{\partial P_{\mathrm{TR}}} = (\lambda_x - e^{-x})\beta w v + \frac{(\lambda_x + \lambda_z e^{-x})\alpha w v c}{[(1-c)P_{\mathrm{TR}} + c]^2} \tag{44}$$

Solving $\partial H/\partial P_{\mathrm{TR}} = 0$, the optimal control is

$$P^*_{\mathrm{TR}}(t) = \left(c \pm \sqrt{\frac{c\alpha[\lambda_x(t) + \lambda_z e^{-x(t)}]}{\beta[e^{-x(t)} - \lambda_x(t)]}} \right) \Big/ (c-1) \tag{45}$$

which is real-valued only if $[e^{-x(t)} - \lambda_x(t)] > 0$. Once again, only the minus root applies. We are also interested in the optimal unconstrained solution, which is

$$P^*_{\mathrm{TR}_u}(t) = \left(c - \sqrt{\frac{c\alpha\lambda_x(t)}{\beta[e^{-x(t)} - \lambda_x(t)]}} \right) \Big/ (c-1) \tag{46}$$

Taking the derivative of Eq. (46) with respect to t gives

$$\dot{P}^*_{\mathrm{TR}_u}(t) = \sqrt{\frac{(wv)^2\alpha\beta e^{-2x(t)}}{4c\lambda_x(t)[e^{-x(t)} - \lambda_x(t)]}}[P^*_{\mathrm{TR}_u}(t)]^2 > 0 \tag{47}$$

Therefore, $P^*_{\mathrm{TR}_u}$ is monotonically increasing and $P^*_{\mathrm{TR}_u}(T) = (c/c-1) > 1$. Thus, the "go for broke" tactic appears again for this unconstrained problem.

Assuming that $c = 100$, $w = 0.2$ (distance), $v = 50$ (distance/time), $\alpha = 10$ (1/distance^2), $\beta = 1$ (1/distance^2), and $T = 0.5$ (time), we solved the constrained problem for a number of $P_{\mathrm{FTA}_{\max}}$ values. Figure 9 shows optimal solutions as a function of time for three values of $P_{\mathrm{FTA}_{\max}}$. Once again, as $P_{\mathrm{FTA}_{\max}}$ decreases, the optimal solution flattens out, approaching a constant-threshold solution.

We compare the objective function values of the dynamic solutions with those of the constant solutions. Figure 10 shows, for the assumed parameters, that the optimal dynamic solution is, at most, 3.6% better than the optimal constant solution. Depending on the application, this improvement may or may not be worth the added complexity. These first two scenarios involved constant ratios of targets to false targets, regardless of the sensor footprint position. The next scenario involves nonconstant ratios of targets to false targets.

IV. Scenario 3: One Normally Distributed Target and a Poisson Field of False Targets

The scenario when one target is normally distributed over a circular battle space among a Poisson field of false targets is now considered. The ratio of targets to false targets depends on the sensor footprint position. The normal distribution is circular, centered at the origin with variance σ^2. The derivation of probabilities is similar to the first scenario, with the following changes. For one normally distributed target,

$$P_{\mathrm{TE}}(r) = \frac{1}{2\pi\sigma^2} e^{-\frac{r^2}{2\sigma^2}} 2\pi r \, \mathrm{d}r \tag{48}$$

The probability of no false-target attacks occurring before reaching radius r is

$$P_{\overline{\mathrm{FTA}}}(r) = e^{-\int_0^r 2\pi[1 - P_{\mathrm{FTR}}(\rho)]\alpha(\rho)\rho \, \mathrm{d}\rho} \tag{49}$$

and the probability of no target attack occurring before reaching radius r is

$$P_{\overline{\mathrm{TA}}}(r) = 1 - \int_0^r \frac{P_{\mathrm{TR}}(\rho)}{\sigma^2} e^{-\frac{\rho^2}{2\sigma^2}} \rho \, \mathrm{d}\rho \tag{50}$$

The probability of a target attack can now be calculated as

$$\begin{aligned} P_{\mathrm{TA}} &= \int_0^R P_{\mathrm{TR}}(r) \cdot P_{\mathrm{TE}}(r) \cdot P_{\overline{\mathrm{FTA}}}(r) \\ &= \int_0^R P_{\mathrm{TR}}(r) \frac{r}{\sigma^2} e^{-\frac{r^2}{2\sigma^2}} \cdot e^{-\int_0^r 2\pi[1 - P_{\mathrm{FTR}}(\rho)]\alpha(\rho)\rho \, \mathrm{d}\rho} \, \mathrm{d}r \end{aligned} \tag{51}$$

and the probability of a false-target attack is

$$\begin{aligned} P_{\mathrm{FTA}} &= \int_0^R [1 - P_{\mathrm{FTR}}(r)] \cdot P_{\mathrm{FTE}}(r) \cdot P_{\overline{\mathrm{TA}}}(r) \cdot P_{\overline{\mathrm{FTA}}}(r) \\ &= \int_0^R [1 - P_{\mathrm{FTR}}(r)] 2\pi r \alpha(r) \\ &\quad \times \left[1 - \int_0^r P_{\mathrm{TR}}(\rho) \frac{\rho}{\sigma^2} e^{-\frac{\rho^2}{2\sigma^2}} \mathrm{d}\rho \right] e^{-\int_0^r 2\pi[1 - P_{\mathrm{FTR}}(\rho)]\alpha(\rho)\rho \, \mathrm{d}\rho} \, \mathrm{d}r \end{aligned} \tag{52}$$

We assume that α is constant.

A. Constant Threshold

If P_{TR} and, consequently, P_{FTR} are constant, we get closed-form solutions when evaluating the integrals in Eqs. (51) and (52). The probability of a target attack is

$$P_{\mathrm{TA}} = \frac{P_{\mathrm{TR}}}{2\sigma^2[(1 - P_{\mathrm{FTR}})\alpha\pi + (1/2\sigma^2)]} (1 - e^{-[(1-P_{\mathrm{FTR}})\alpha\pi + \frac{1}{2\sigma^2}]R^2}) \tag{53}$$

and the probability of a false-target attack is

$$P_{\mathrm{FTA}} = 1 - P_{\mathrm{TA}} - (1 - P_{\mathrm{TR}} + P_{\mathrm{TR}} e^{\frac{-R^2}{2\sigma^2}}) e^{-(1-P_{\mathrm{FTR}})\alpha\pi R^2} \tag{54}$$

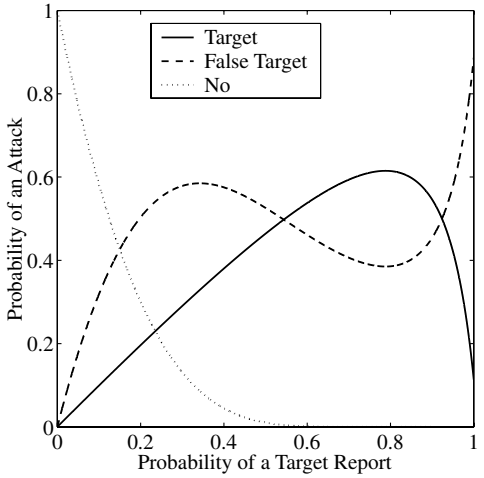

Fig. 11 Scenario involves a normally distributed target and a Poisson field of false targets; probability of a target report is constant throughout the flight; $c = 100$, $\alpha = 5$ (1/distance^2), $\sigma^2 = 0.25$ (distance^2), and $R = 5$ (distance).

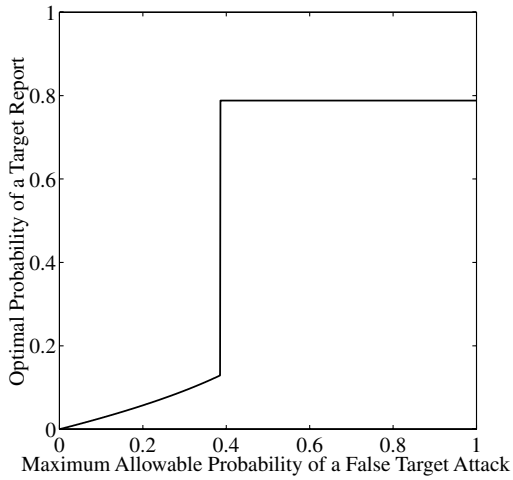

Fig. 12 Scenario involves a normally distributed target and a Poisson field of false targets; probability of a target report is constant throughout the flight; $c = 100$, $\alpha = 5$ (1/distance^2), $\sigma^2 = 0.25$ (distance^2), and $R = 5$ (distance).

To show an example, values must be provided for the various constants; units are distance units. Invoking the ROC model in Eq. (1) and assuming that $c = 100$, $\alpha = 5$ (1/distance^2), $\sigma^2 = 0.25$ (distance^2), and $R = 5$ (distance), we plot the outcome probabilities versus P_{TR}. Figure 11 shows that the best unconstrained solution is $P^*_{\mathrm{TR}_u} = 0.788$ with a corresponding $P^*_{\mathrm{TA}_u} = 0.615$ and $P^*_{\mathrm{FTA}_u} = 0.385$. If we bound P_{FTA} by $P_{\mathrm{FTA}_{\max}} = 0.20$, the best constrained solution is $P^*_{\mathrm{TR}} = 0.057$ with a corresponding $P^*_{\mathrm{TA}} = 0.057$. This is a significant reduction in performance.

Like the scenario with one uniformly distributed target, the function for P_{TA} has one peak and never crosses the line when $P_{\mathrm{TA}} = P_{\mathrm{TR}}$. However, as a result of the changing ratio of targets to false targets, the function for P_{FTA} is not necessarily increasing. Figure 11 shows that P_{FTA} increases, then decreases, then increases again. For values of P_{FTA} above the local minimum at $P_{\mathrm{FTA}} = 0.385$, the unconstrained solution is used. On a plot of P^*_{TR} versus $P_{\mathrm{FTA}_{\max}}$, a discontinuous jump appears, as shown in Fig. 12.

B. Dynamic Threshold

When P_{TR} and, consequently, P_{FTR} are dynamic, the state variables become

$$x = \int_0^r 2\pi\alpha\rho[1 - P_{\mathrm{FTR}}(\rho)]\,\mathrm{d}\rho \tag{55}$$

$$y = \int_0^r P_{\mathrm{TR}}(\rho)\frac{\rho}{\sigma^2}e^{-\frac{\rho^2}{2\sigma^2}}\,\mathrm{d}\rho \tag{56}$$

$$z = \int_0^r 2\pi\alpha\rho[1 - P_{\mathrm{FTR}}(\rho)][1 - y(\rho)]e^{-x(\rho)}\,\mathrm{d}\rho \tag{57}$$

and define L as

$$L = -P_{\mathrm{TR}}(r)\frac{r}{\sigma^2}e^{-\frac{r^2}{2\sigma^2}}e^{-x(r)} \tag{58}$$

The state equations are

$$\dot{x} = 2\pi\alpha r[1 - P_{\mathrm{FTR}}(r)] \tag{59}$$

$$\dot{y} = P_{\mathrm{TR}}(r)\frac{r}{\sigma^2}e^{-\frac{r^2}{2\sigma^2}} \tag{60}$$

$$\dot{z} = 2\pi\alpha r[1 - P_{\mathrm{FTR}}(r)][1 - y(r)]e^{-x(r)} \tag{61}$$

After applying Eq. (1) for the ROC model, the Hamiltonian becomes

$$H = (\lambda_y - e^{-x})P_{\mathrm{TR}}(r)\frac{r}{\sigma^2}e^{-\frac{r^2}{2\sigma^2}} + 2\pi\alpha r\frac{P_{\mathrm{TR}}}{(1-c)P_{\mathrm{TR}} + c}[\lambda_x + \lambda_z(1-y)e^{-x}] \tag{62}$$

and the costate differential equations become

$$\dot{\lambda}_x = \lambda_z 2\pi\alpha r\frac{P_{\mathrm{TR}}}{(1-c)P_{\mathrm{TR}} + c}(1-y)e^{-x} - P_{\mathrm{TR}}(r)\frac{r}{\sigma^2}e^{-\frac{r^2}{2\sigma^2}}e^{-x} \tag{63}$$

$$\dot{\lambda}_y = \lambda_z 2\pi\alpha r\frac{P_{\mathrm{TR}}}{(1-c)P_{\mathrm{TR}} + c}e^{-x} \tag{64}$$

$$\dot{\lambda}_z = 0 \tag{65}$$

Taking the partial derivative of H with respect to the decision variable P_{TR} gives

$$\frac{\partial H}{\partial P_{\mathrm{TR}}} = (\lambda_y - e^{-x})\frac{r}{\sigma^2}e^{-\frac{r^2}{2\sigma^2}} + \frac{[\lambda_x + \lambda_z(1-y)e^{-x}]2\pi\alpha rc}{[(1-c)P_{\mathrm{TR}} + c]^2} \tag{66}$$

Solving $\partial H/\partial P_{\mathrm{TR}} = 0$, the optimal control is

$$P^*_{\mathrm{TR}}(r) = \left(c \pm \sqrt{\frac{\{\lambda_x(r) + \lambda_z[1-y(r)]e^{-x(r)}\}2\pi\alpha c\sigma^2 e(r^2/2\sigma^2)}{[e^{-x(r)} - \lambda_y(r)]}}\right)\Big/(c-1) \tag{67}$$

Once again, only the minus root is used. One is also interested in the optimal unconstrained solution, which is

$$P^*_{\mathrm{TR}_u}(r) = \frac{c - \sqrt{\lambda_x(r)2\pi\alpha c\sigma^2 e^{[x(r) + \frac{r^2}{2\sigma^2}]}}}{c-1} \tag{68}$$

Taking the derivative of Eq. (68) with respect to r gives

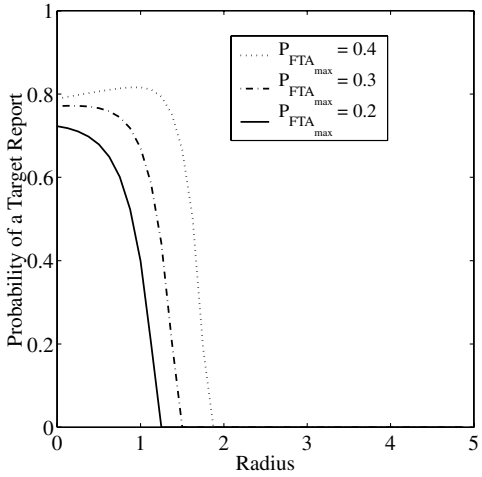

Fig. 13 Scenario involves a normally distributed target and a Poisson field of false targets; $c = 100$, $\alpha = 5$ (1/distance^2), $\sigma^2 = 0.25$ (distance^2), and $R = 5$ (distance).

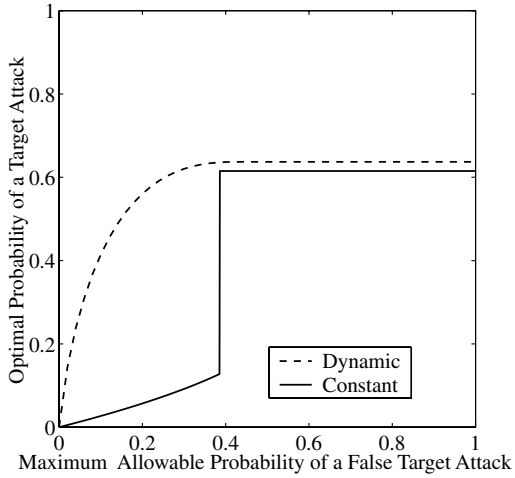

Fig. 14 Scenario involves a normally distributed target and a Poisson field of false targets; $c = 100$, $\alpha = 5$ (1/distance^2), $\sigma^2 = 0.25$ (distance^2), and $R = 5$ (distance).

$$\dot{P}^*_{\mathrm{TR}_u}(r) = -\sqrt{\frac{2\pi\alpha c r^2}{4(c-1)^2\sigma^2\lambda_x(r)e^{\left[x(r)+\frac{r^2}{2\sigma^2}\right]}}} \times \left\{\lambda_x(r)e^{\left[x(r)+\frac{r^2}{2\sigma^2}\right]} - \frac{(c-1)}{c}[P^*_{\mathrm{TR}_u}(r)]^2\right\} \tag{69}$$

Unlike the previous scenarios, it is unclear whether $P^*_{\mathrm{TR}_u}$ is increasing or decreasing.

Assuming that $c = 100$, $\alpha = 5$ (1/distance^2), $\sigma^2 = 0.25$ (distance^2), and $R = 5$ (distance), we solved the constrained problem for a number of $P_{\mathrm{FTA}_{\max}}$ values. Figure 13 shows that as $P_{\mathrm{FTA}_{\max}}$ decreases, the sensor is turned off earlier in the search.

We compare the objective function values of the dynamic solutions to those of the constant solutions. Figure 14 shows the poor performance of the constant-threshold solution when $P_{\mathrm{FTA}_{\max}} < 0.385$. Unlike the previous two scenarios in which dynamic-threshold solutions were only a few percent better than constant-threshold solutions, there are substantial improvements when $P_{\mathrm{FTA}_{\max}} < 0.385$. Because the dynamic problem allows the sensor to be turned off at some point, the solutions are similar to those at smaller R values. In essence, one learns how far out in the radius to search. The dynamic problem "recognizes" the benefit of staying close to the origin when a target is normally distributed. The constant-parameter problem forces one to arbitrarily pick R and then optimize P_{TR} based on R. Thus, we must settle for poor performance when R is chosen too large.

V. Conclusions

Three scenarios were considered involving an airborne munition searching for stationary targets among a field of false targets. Targets were modeled using uniform, Poisson, and normal distributions. False targets were modeled using Poisson distributions. The control variable was the probability of a target report, which is linked to the probability of a false-target report via the sensor's receiver operating characteristic curve. Optimization problems were formulated that maximize the probability of a target attack while constraining the probability of a false-target attack. Generalized expressions for these two probabilities were derived for all three scenarios. Both constant- and dynamic-threshold solutions were given for a sample instance of each scenario. For the two scenarios involving constant target-to-false-target ratios, the optimal dynamic threshold was only a few percent better than the best constant threshold. For the scenario in which the target-to-false-target ratio changed during the search, the optimal dynamic threshold was substantially better than the optimal constant threshold.

Future work will include parameterizing receiver operating characteristic curves by area coverage rate and formulating problems for air vehicles with multiple warheads. These generalizations will open the solution space to planar regions and expand the applications to unmanned combat air vehicles and general sensor craft. As autonomous unmanned vehicles become increasingly prevalent in combat environments, more basic research involving analytic effectiveness measures (such as the work presented here) is needed.

A. Appendix: Probability Derivations

We derive formulas for probabilities of events when parameters vary with time or space. Specifically, we are interested in the probability of no target attacks and the probability of no false-target attacks before a time t or radius r. For example, no target attacks happen if no targets were encountered or all targets encountered were misclassified. We denote by P_c a general classification probability that can assume the role of P_{TR}, $1 - P_{\mathrm{TR}}$, P_{FTR}, or $1 - P_{\mathrm{FTR}}$, depending on the application. Events involving only encounters are denoted as $\mathcal{E}$, and events involving classified encounters are denoted as $\mathcal{C}$. The number of events occurring in a given area is subscripted, along with the applicable area; for example, one classified encounter in ΔA_1 is denoted as $\mathcal{C}_{1,\Delta A_1}$.

I. Uniform Distribution

We consider the case of searching for one uniformly distributed target. The air vehicle flies a straight path, as illustrated in Fig. 1; however, its classification probabilities, search width, and velocity are not constant, but are allowed to vary with time. The probability of no encounters (and hence no classification) during $[0, t]$ is

$$P(\mathcal{E}_{0,A}) = 1 - \frac{1}{A_s}\int_0^t w(\tau)v(\tau)\,\mathrm{d}\tau \tag{A1}$$

where

$$A_s = \int_0^T w(\tau)v(\tau)\,\mathrm{d}\tau \tag{A2}$$

To calculate the probability of exactly one classified encounter occurring during $[0, t]$, divide the time interval into n short time periods of length $\tau_1, \ldots, \tau_n$ such that

$$\sum_{i=1}^{n}\tau_i = t \tag{A3}$$

Let the mean probability of classification, search width, and velocity in the ith interval be P_{c_i}, w_i, and v_i, respectively. The incremental area is given by

$$\Delta A_i = w_i v_i \tau_i \tag{A4}$$

and the search area is given

$$A_s = \sum_i^n \Delta A_i \tag{A5}$$

The probability of exactly one classified encounter occurring during $[0, t]$ requires considering all the permutations in which one classified encounter could occur; that is,

$$P(\mathcal{C}_{1,A}) = P(\mathcal{C}_{1,\Delta A_1}) + P(\mathcal{C}_{1,\Delta A_2}) + \cdots + P(\mathcal{C}_{1,\Delta A_n}) \tag{A6}$$

so

$$\begin{aligned} P(\mathcal{C}_{1,A}) &= \frac{w_1 v_1 \tau_1}{A_s} P_{c_1} + \frac{w_2 v_2 \tau_2}{A_s} P_{c_2} + \cdots + \frac{w_n v_n \tau_n}{A_s} P_{c_n} \\ &= \frac{1}{A_s} \sum_{i=1}^n w_i v_i \tau_i P_{c_i} \end{aligned} \tag{A7}$$

Taking the limit as $\tau_i \to 0$, $i = 1, \ldots, n$, $n \to \infty$ such that

$$\sum_{i=1}^n \tau_i = t$$

we get

$$P(\mathcal{C}_{1,A}) = \frac{1}{A_s} \int_0^t P_c(\tau) w(\tau) v(\tau)\, \mathrm{d}\tau \tag{A8}$$

We now calculate the joint probability of no encounters and one classified encounter during $[0, t]$. The two events are mutually exclusive, thus one must sum the two individual probabilities:

$$\begin{aligned} P(\mathcal{E}_{0,A} \cap \mathcal{C}_{1,A}) &= 1 - \frac{1}{A_s} \int_0^t w(\tau) v(\tau)\, \mathrm{d}\tau + \frac{1}{A_s} \int_0^t P_c(\tau) w(\tau) v(\tau)\, \mathrm{d}\tau \\ &= 1 - \frac{1}{A_s} \int_0^t [1 - P_c(\tau)] w(\tau) v(\tau)\, \mathrm{d}\tau \end{aligned} \tag{A9}$$

For the probability of no target attack before time t, Eq. (A9) is used with $P_c(\tau) = 1 - P_{\mathrm{TR}}(\tau)$, giving

$$P_{\overline{\mathrm{TA}}}(t) = 1 - \frac{1}{A_s} \int_0^t P_{\mathrm{TR}}(\tau) w(\tau) v(\tau)\, \mathrm{d}\tau \tag{A10}$$

II. Poisson Distribution

Let $\mu(\tau)$ be the rate of encounters at time τ. Divide the time interval $[0, t]$ into n short time periods of length $\tau_1, \ldots, \tau_n$ such that

$$\sum_{i=1}^n \tau_i = t \tag{A11}$$

Let the mean rate of occurrence for target encounters and mean probability of classification in the ith interval be μ_i and P_{c_i}, respectively. The standard Poisson probability law requires, "If an area is subdivided into n subareas and for $i = 1, \ldots, n$, E_i denotes the event that at least one or more encounters occur in the ith subarea, then, for any integer n, $E_1, \ldots, E_n$ are independent events" [1]. Hence, the probability that exactly j_i encounters occur in the interval τ_i, $i = 1, \ldots, n$ is

$$P(j_1, \ldots, j_n) = \prod_{i=1}^n e^{-\mu_i \tau_i} \frac{(\mu_i \tau_i)^{j_i}}{j_i!} = e^{-\sum_{i=1}^n \mu_i \tau_i} \prod_{i=1}^n \frac{(\mu_i \tau_i)^{j_i}}{j_i!} \tag{A12}$$

The probability of no encounters occurring (and hence no classification) during $[0, t]$ is

$$P(\mathcal{E}_{0,A}) = e^{-\sum_{i=1}^n \mu_i \tau_i} \tag{A13}$$

Let $j = 1$. The probability of one classified encounter in the ith interval is

$$P(\mathcal{C}_{1,\Delta A_i}) = e^{-\sum_{i=1}^n \mu_i \tau_i} \frac{(\mu_i \tau_i)^1}{1!} P_{c_i} \tag{A14}$$

The probability of exactly one classified encounter occurring during $[0, t]$ requires considering all the permutations in which one classified encounter could occur; that is,

$$P(\mathcal{C}_{1,A}) = P(\mathcal{C}_{1,\Delta A_1}) + P(\mathcal{C}_{1,\Delta A_2}) + \cdots + P(\mathcal{C}_{1,\Delta A_n}) \tag{A15}$$

So

$$\begin{aligned} P(\mathcal{C}_{1,A}) &= e^{-\sum_{i=1}^n \mu_i \tau_i} \frac{(\mu_1 \tau_1)^1}{1!} P_{c_1} \\ &\quad + e^{-\sum_{i=1}^n \mu_i \tau_i} \frac{(\mu_2 \tau_2)^1}{1!} P_{c_2} + \cdots + e^{-\sum_{i=1}^n \mu_i \tau_i} \frac{(\mu_n \tau_n)^1}{1!} P_{c_n} \\ &= e^{-\sum_{i=1}^n \mu_i \tau_i} \sum_{i=1}^n \mu_i \tau_i P_{c_i} \end{aligned} \tag{A16}$$

The probability of exactly two classified encounters occurring during $[0, t]$ requires considering all the permutations in which two classified encounters could occur; that is,

$$\begin{aligned} P(\mathcal{C}_{2,A}) &= P(\mathcal{C}_{1,\Delta A_1} \cap \mathcal{C}_{1,\Delta A_2}) + P(\mathcal{C}_{1,\Delta A_1} \cap \mathcal{C}_{1,\Delta A_3}) + \cdots \\ &\quad + P(\mathcal{C}_{1,\Delta A_1} \cap \mathcal{C}_{1,\Delta A_n}) + P(\mathcal{C}_{1,\Delta A_2} \cap \mathcal{C}_{1,\Delta A_3}) \\ &\quad + P(\mathcal{C}_{1,\Delta A_2} \cap \mathcal{C}_{1,\Delta A_4}) + \cdots + P(\mathcal{C}_{1,\Delta A_2} \cap \mathcal{C}_{1,\Delta A_n}) + \cdots \\ &\quad + P(\mathcal{C}_{1,\Delta A_{n-1}} \cap \mathcal{C}_{1,\Delta A_n}) + P(\mathcal{C}_{2,\Delta A_1}) \\ &\quad + P(\mathcal{C}_{2,\Delta A_2}) + \cdots + P(\mathcal{C}_{2,\Delta A_n}) \end{aligned} \tag{A17}$$

So

$$\begin{aligned} P(\mathcal{C}_{2,A}) &= e^{-\sum_{i=1}^n \mu_i \tau_i} \frac{(\mu_1 \tau_1)^1}{1!} P_{c_1} \\ &\quad \times \left[\frac{(\mu_2 \tau_2)^1}{1!} P_{c_2} + \cdots + \frac{(\mu_n \tau_n)^1}{1!} P_{c_n} \right] \\ &\quad + e^{-\sum_{i=1}^n \mu_i \tau_i} \frac{(\mu_2 \tau_2)^1}{1!} P_{c_2} \left[\frac{(\mu_3 \tau_3)^1}{1!} P_{c_3} + \cdots + \frac{(\mu_n \tau_n)^1}{1!} P_{c_n} \right] \\ &\quad + \cdots e^{-\sum_{i=1}^n \mu_i \tau_i} \frac{(\mu_{n-1} \tau_{n-1})^1}{1!} P_{c_{n-1}} \frac{(\mu_n \tau_n)^1}{1!} P_{c_n} \\ &\quad + e^{-\sum_{i=1}^n \mu_i \tau_i} \left[\frac{(\mu_1 \tau_1)^2}{2!} P_{c_1}^2 + \cdots + \frac{(\mu_n \tau_n)^2}{2!} P_{c_n}^2 \right] \\ &\quad = \frac{1}{2} e^{-\sum_{i=1}^n \mu_i \tau_i} [2 \mu_1 \tau_1 P_{c_1} (\mu_2 \tau_2 P_{c_2} + \cdots + \mu_n \tau_n P_{c_n}) \\ &\quad + 2 \mu_2 \tau_2 P_{c_2} (\mu_3 \tau_3 P_{c_3} + \cdots + \mu_n \tau_n P_{c_n}) + \cdots \\ &\quad + 2 \mu_{n-1} \tau_{n-1} P_{c_{n-1}} \mu_n \tau_n P_{c_n} + (\mu_1 \tau_1 P_{c_1})^2 + (\mu_2 \tau_2 P_{c_2})^2 + \cdots \\ &\quad + (\mu_n \tau_n P_{c_n})^2] \\ &\quad = e^{-\sum_{i=1}^n \mu_i \tau_i} \frac{(\sum_{i=1}^n \mu_i \tau_i P_{c_i})^2}{2} \end{aligned} \tag{A18}$$

In general, the probability of exactly j classified encounters occurring during $[0, t]$ is

$$P(\mathcal{C}_{j,A}) = e^{-\sum_{i=1}^n \mu_i \tau_i} \frac{(\sum_{i=1}^n \mu_i \tau_i P_{c_i})^j}{j!} \tag{A19}$$

Taking the limit as $\tau_i \to 0$, $i = 1, \ldots, n$, $n \to \infty$ such that

$$\sum_{i=1}^n \tau_i = t$$

yields

$$P(\mathcal{C}_{j,A}) = e^{-\int_0^t \mu(\tau)\,\mathrm{d}\tau} \frac{[\int_0^t P_c(\tau)\mu(\tau)\,\mathrm{d}\tau]^j}{j!} \tag{A20}$$

We can use Eq. (A20) to determine the probability of either no false-target attacks or no target attacks occurring up through time t. In the case of no false-target attacks, the possible mutually exclusive events are from no encounters, to one encounter correctly classified, through an infinite number of encounters correctly classified. Thus,

$$\begin{aligned}
&P(\mathcal{E}_{0,A} \cap \mathcal{C}_{1,A} \cap \ldots \cap \mathcal{C}_{\infty,A}) = P(\mathcal{E}_{0,A}) + P(\mathcal{C}_{1,A}) + \cdots + P(\mathcal{C}_{\infty,A}) \\
&= e^{-\int_0^t \mu(\tau)\,\mathrm{d}\tau} + e^{-\int_0^t \mu(\tau)\,\mathrm{d}\tau} \frac{[\int_0^t P_c(\tau)\mu(\tau)\,\mathrm{d}\tau]^1}{1!} \\
&+ \cdots + e^{-\int_0^t \mu(\tau)\,\mathrm{d}\tau} \frac{[\int_0^t P_c(\tau)\mu(\tau)\,\mathrm{d}\tau]^\infty}{\infty!} \\
&= e^{-\int_0^t \mu(\tau)\,\mathrm{d}\tau} \left[1 + \frac{[\int_0^t P_c(\tau)\mu(\tau)\,\mathrm{d}\tau]^1}{1!} + \cdots + \frac{[\int_0^t P_c(\tau)\mu(\tau)\,\mathrm{d}\tau]^\infty}{\infty!}\right] \\
&= e^{-\int_0^t \mu(\tau)\,\mathrm{d}\tau} e^{\int_0^t P_c(\tau)\mu(\tau)\,\mathrm{d}\tau} \\
&= e^{-\int_0^t [1-P_c(\tau)]\mu(\tau)\,\mathrm{d}\tau}
\end{aligned} \tag{A21}$$

To calculate the probability of no false-target attacks, let $P_c(\tau) = P_{\mathrm{FTR}}(\tau)$ and $\mu(\tau) = \alpha(\tau)w(\tau)v(\tau)$ in Eq. (A21), giving

$$P_{\overline{\mathrm{FTA}}}(t) = e^{-\int_0^t [1-P_{\mathrm{FTR}}(\tau)]\alpha(\tau)w(\tau)v(\tau)\,\mathrm{d}\tau} \tag{A22}$$

where $\alpha(\tau)$ is the false-target density. To calculate the probability of no target attacks, we let $P_c(\tau) = 1 - P_{\mathrm{TR}}(\tau)$ and $\mu(\tau) = \beta(\tau)w(\tau)v(\tau)$ in Eq. (A21), giving

$$P_{\overline{\mathrm{TA}}}(t) = e^{-\int_0^t [P_{\mathrm{TR}}(\tau)]\beta(\tau)w(\tau)v(\tau)\,\mathrm{d}\tau} \tag{A23}$$

where $\beta(\tau)$ is the target density. The integrals in Eq. (A22) and (A23) serve as Poisson parameters, which are assumed constant in the literature. We define these integrals as *dynamic Poisson parameters*. When formulating optimal control problems, the integrals are defined as stated.

III. Normal Distribution

We consider the case of searching for one normally distributed target in a circular disc of radius r. Normally distributed refers to circular normal distribution with standard deviation σ. The classification probabilities vary with radius. The probability of no encounters (and hence no classification) searching a disc of radius r from the origin outward using concentric annuli of thickness $\mathrm{d}\rho$ is

$$\begin{aligned}
P(\mathcal{E}_{0,A}) &= 1 - \int_0^{2\pi} \int_0^r \frac{1}{2\pi\sigma^2} e^{-\frac{\rho^2}{2\sigma^2}} \rho\,\mathrm{d}\rho\,\mathrm{d}\theta \\
&= 1 - \int_0^r \frac{1}{\sigma^2} e^{-\frac{\rho^2}{2\sigma^2}} \rho\,\mathrm{d}\rho
\end{aligned} \tag{A24}$$

To calculate the probability of one classified encounter, divide the disc of area A into n concentric annuli of area $A_1, \ldots, A_n$ such that

$$\sum_{i=1}^{n} A_i = A \tag{A25}$$

Each A_i is calculated using

$$A_i = 2\pi\rho_i \Delta\rho_i \tag{A26}$$

where ρ_i is the radius of the annulus and $\Delta\rho_i$ is the thickness. The search begins at the origin of the disc and progresses outward such that $\rho_i < \rho_{i+1}$ and $i = 1, \ldots, n-1$. Let the mean probability of classification in the ith annulus be P_{c_i}. The probability of one classified encounter during the sweep of A requires considering all the permutations in which one classified encounter could occur; that is

$$P(\mathcal{C}_{1,A}) = P(\mathcal{C}_{1,\Delta A_1}) + P(\mathcal{C}_{1,\Delta A_2}) + \cdots + P(\mathcal{C}_{1,\Delta A_n}) \tag{A27}$$

So

$$\begin{aligned}
P(\mathcal{C}_{1,A}) &= 2\pi\rho_1\Delta\rho_1 \frac{1}{2\pi\sigma^2} e^{-\frac{\rho_1^2}{2\sigma^2}} P_{c_1} + \cdots + 2\pi\rho_n\Delta\rho_n \frac{1}{2\pi\sigma^2} e^{-\frac{\rho_n^2}{2\sigma^2}} P_{c_n} \\
&= \sum_{i=1}^{n} \frac{1}{\sigma_2} \rho_i \Delta\rho_i e^{-\frac{\rho_i^2}{2\sigma^2}} P_{c_i}
\end{aligned} \tag{A28}$$

Taking the limit as $\Delta\rho_i \to 0$, $i = 1, \ldots, n$, and $n \to \infty$ such that

$$\sum_{i=1}^{n} A_i = A$$

we get

$$P(\mathcal{C}_{1,A}) = \int_0^r \frac{P_c(\rho)}{\sigma^2} e^{-\frac{\rho^2}{2\sigma^2}} \rho\,\mathrm{d}\rho \tag{A29}$$

We now calculate the joint probability of no encounters and one classified encounter during the sweep of A. The two events are mutually exclusive, thus one must sum the two individual probabilities:

$$\begin{aligned}
P(\mathcal{E}_{0,A} \cap \mathcal{C}_{1,A}) &= 1 - \int_0^r \frac{1}{\sigma^2} e^{-\frac{\rho^2}{2\sigma^2}} \rho\,\mathrm{d}\rho + \int_0^r \frac{P_c(\rho)}{\sigma^2} e^{-\frac{\rho^2}{2\sigma^2}} \rho\,\mathrm{d}\rho \\
&= 1 - \int_0^r \frac{[1 - P_c(\rho)]}{\sigma^2} e^{-\frac{\rho^2}{2\sigma^2}} \rho\,\mathrm{d}\rho
\end{aligned} \tag{A30}$$

For the probability of no target attack before radius r, Eq. (A30) is used with $P_c(\rho) = 1 - P_{\mathrm{TR}}(\rho)$, giving

$$P_{\overline{\mathrm{TA}}}(r) = 1 - \int_0^r \frac{P_{\mathrm{TR}}(\rho)}{\sigma^2} e^{-\frac{\rho^2}{2\sigma^2}} \rho\,\mathrm{d}\rho \tag{A31}$$

References

[1] Jacques, D. R., and Pachter, M., "A Theoretical Foundation for Cooperative Search, Classification, and Target Attack," *Cooperative Control: Models, Applications and Algorithms*, Kluwer Academic, Norwell, MA, 2004.

[2] Koopman, B. O., *Search and Screening*, Pergamon, New York, 1980.

[3] Washburn, A. R., *Search and Detection*, Topics in Operations Research Series, Operations Research Society of America, Arlington, VA, 1981.

[4] Moses, L. E., Shapiro, D. E., and Littenberg, B., "Combining Independent Studies of a Diagnostic Test into a Summary ROC Curve: Data-Analytic Approaches and Some Additional Considerations," *Statistics in Medicine*, Vol. 12, Wiley, New York, 1993.

[5] Bryson, A. E., and Ho, Y., *Applied Optimal Control*, Ginn, Waltham, MA, 1969.

[6] Bryson, A. E., *Dynamic Optimization*, Addison Wesley Longman, Reading, MA, 1999.